



Missouri University of Science and Technology
Scholars' Mine

Mathematics and Statistics Faculty Research &
Creative Works

Mathematics and Statistics

7-1-2019

On the Instabilities and Transitions of the Western Boundary Current


Daozhi Han

Missouri University of Science and Technology, handaoz@mst.edu

Marco Hernandez

Quan Wang

Follow this and additional works at: https://scholarsmine.mst.edu/math_stat_facwork

 Part of the [Mathematics Commons](#), and the [Statistics and Probability Commons](#)

Recommended Citation

D. Han et al., "On the Instabilities and Transitions of the Western Boundary Current," *Communications in Computational Physics*, vol. 26, no. 1, pp. 35-56, Global-Science Press, Jul 2019.

The definitive version is available at <https://doi.org/10.4208/cicp.OA-2018-0066>

This Article - Journal is brought to you for free and open access by Scholars' Mine. It has been accepted for inclusion in Mathematics and Statistics Faculty Research & Creative Works by an authorized administrator of Scholars' Mine. This work is protected by U. S. Copyright Law. Unauthorized use including reproduction for redistribution requires the permission of the copyright holder. For more information, please contact scholarsmine@mst.edu.

On the Instabilities and Transitions of the Western Boundary Current

Daozhi Han^{1,*}, Marco Hernandez² and Quan Wang³

¹ *Missouri University of Science and Technology, 400 W. 12th. St, Rolla, MO, 65409, USA.*

² *Department of Mathematics, Indiana University, Bloomington, IN 47405, USA.*

³ *Department of Mathematics, Sichuan University, Chengdu, China.*

Received 15 March 2018; Accepted (in revised version) 12 June 2018

Abstract. We study the stability and dynamic transitions of the western boundary currents in a rectangular closed basin. By reducing the infinite dynamical system to a finite dimensional one via center manifold reduction, we derive a non-dimensional transition number that determines the types of dynamical transition. We show by careful numerical evaluation of the transition number that both continuous transitions (supercritical Hopf bifurcation) and catastrophic transitions (subcritical Hopf bifurcation) can happen at the critical Reynolds number, depending on the aspect ratio and stratification. The regions separating the continuous and catastrophic transitions are delineated on the parameter plane.

AMS subject classifications: 37D45, 35Q99, 34C23, 76U05, 76D03

Key words: Western boundary current, dynamic transition, instability, Hopf bifurcation, spectral method.

1 Introduction

Wind-driven circulation/currents and their variability is a central theme in the study of climate dynamics and oceanography. See [10] for a recent comprehensive review of the survey of wind-driven circulation from the perspective of dynamical systems theory. One of the strongest near-surface, mid-latitude currents is the Gulf stream [28]. This current intensifies along the western shores of the North Atlantic (east coast of North America), exhibiting boundary layer characteristics with an intense crowding of the streamlines, and is commonly referred to as the western boundary current. The western boundary currents, which are of intense shear flows, are subject to internal instabilities. In this

*Corresponding author. *Email addresses:* handaoz@mst.edu (D. Han), hernmarc@indiana.edu (M. Hernandez), wqxihu junzi@126.com (Q. Wang)

article, we aim to theoretically and numerically study the variability and dynamical transitions of the western boundary currents in a rectangular closed basin.

The study of the western boundary currents has a long history. Earlier works on this topic are mainly done by physicists relying on either analytical solutions of simplified models or purely numerical simulation. Stommel first studies the western boundary currents in the linear regime and discovers that the variation of the Coriolis effect with latitude is the physical mechanism behind the intense currents. Munk in [20] proposes another linear model and finds an analytical solution known as the Munk boundary layer profile that represents a concentrated current like the Gulf stream. The boundary layer analysis of a nonlinear model and the numerical integration can be found in [2, 29, 30] by Veronis. These early results, cf. in particular [4], already suggest that, for the Rossby number in the geophysical regime, there is a critical Reynolds number below which a steady-state solution is approached asymptotically, while shear flow instabilities develop after the transition.

Ierley and Young in [11] study the linear instabilities of a family of basic states including the Munk profile in the western boundary currents by numerically solving a modified Orr-Sommerfeld equation. It is found that the critical Reynolds number at which the basic states become unstable is relatively low (between 20 to 100) and that the unstable modes are trapped in the boundary layer with a slowly varying oscillatory tail. A systematic numerical investigation of the linear instabilities of the western boundary current is carried out by Berloff and Meacham in [3], and by Berloff and McWilliams in [1] for both no-slip and free-slip boundary conditions. Their numerical method is based on the theory of dynamical systems that a change in the stability properties of a steady-state solution will lead to a change in the nature of the solution to which the model asymptotes at a considerable time. By examining carefully the asymptotics of the numerical solution at varying Reynolds number, they only find supercritical Hopf bifurcations in which the amplitudes of the bifurcated limit cycles tend to zero as the critical Reynolds number is approached from the unstable side, though in reality, as we show in this article, subcritical Hopf bifurcations are also possible for certain parameter values. Similar numerical results are also reported in [12, 13]. Mathematically, the existence of bifurcating periodic solutions in a quasi-geostrophic model of wind-driven circulation is investigated by Chen and Price in [6], see also [5]. We refer to the review articles [8, 10] and references therein for the detailed bifurcation analysis of general circulation models.

Previous works on the instabilities of the western boundary currents and the resulting formation of periodic vortices are limited by the scope of the numerical investigation in the presence of multiple control parameters. In this article, we tackle this problem from the perspective of the dynamic transition theory developed by Ma and Wang [18] which is entirely different from previous researches. The main philosophy of this theory is to search for the full set of transition states, giving a complete characterization of stability and transition. The set of transition states can be represented by a local attractor. Following this philosophy, the dynamic transition theory aims to identify the transition states and to classify them both dynamically and physically. One important ingredient

of the theory is the introduction of a new classification scheme of transitions, with which phase transitions are classified into three types: continuous, catastrophic, and random. Roughly speaking, a continuous transition means that the basic state bifurcates to a local attractor; a catastrophic transition means that a system will jump to another state, and a random transition indicates that both continuous and catastrophic transitions are possible depending on the initial perturbation. The theory has been successfully applied in the study of a number of transition problems, including transitions of quasi-geostrophic channel flows [7], instability and transitions of Rayleigh-Benard convection [16, 23, 24], dynamic transitions of Cahn-Hilliard equation [14, 15], boundary layer separation [17], see also [21, 31]. In this article, we show that the type of the transition of the western boundary currents, represented by the Munk boundary layer profile in the quasi-geostrophic circulation model, can be uniquely determined by the sign of a parameter, called transition number whose value can be efficiently computed numerically.

The major part of this work is dedicated to the center manifold reduction under the condition of Principle of Exchange of Stability that is established by earlier works on linear stability analysis. That is, we reduce the original system of partial differential equations to a system of ordinary differential equations on the center manifold generated by the unstable modes at the critical Reynolds number. The dynamic transition is then studied via the reduced system following the ideas from the dynamic transition theory. The transition number signifying types of dynamical transitions is derived from the reduced equations. Numerical evaluations of the transition number demonstrate that both continuous transitions (supercritical Hopf bifurcation) and catastrophic transitions (subcritical Hopf bifurcation) can happen at the critical Reynolds number, depending on the stratification and the aspect ratio of the basin. Thus our result gives a complete characterization of the formation of periodic vortices as a result of the dynamic transition of the western boundary currents at the first critical Reynolds number.

The rest of this paper is organized as follows. In Section 2, we introduce the governing equations and the basic flow. The linear stability analysis and the Principle of Exchange of Stability condition (PES) is pursued in Section 3. The main transition theorem and its proof is presented in Section 4. In Section 5 we outline a Legendre-spectral numerical procedure for computing the transition number and illustrate different types of transitions depending on the parameters of stratification and aspect ratio of the basin. We conclude the article with a summary in Section 6.

2 Governing equation

The mechanism of instability for the western boundary currents is rather complicated. In this article we focus exclusively on the viscous instability of the western boundary currents governed by a simplified quasi-geostrophic (QG) reduced gravity model, cf. [2, 3]. We restrict our study to a rectangular basin of the midlatitudes with x being in the west-east direction and y in the south-north direction after the β -plane approximation, see

the monographs [19, 22]. As in [2], we neglect the mechanism of bottom topography and thermohaline effects of the ocean, instead adopt a 1.5-layer model of stratification where an upper active layer is superimposed over a static lower layer of infinite depth. The density difference of the two layers will be represented by a reduced gravitational constant. We make a further simplification in the model: the basin is assumed to be narrow so that the wind stress is uniform in y and periodic boundary condition is imposed in the y -direction. This simplification leads to a modified Orr-Sommerfeld eigenvalue problem for linear stability analysis, which is convenient for numerical investigation. The scales in our model represent roughly those of the Black Sea, cf. [2]. We point out that the physical problem of instability associated with the western boundary currents are intrinsically multi-dimension. It is our hope that the results derived from the simplified model bear physical relevance to the instability and transition of the western boundary currents in real world. The analytical approach of dynamical transition theory we undertake here is still applicable in the general setting, though a robust numerical procedure capable of dealing with high-dimensional data (eigenvalue problems by PDEs with multiple parameters) needs to be developed.

In the setting outlined above, we adopt the Equivalent Barotropic (EB) model as a simplification for the motion of the western boundary currents in a rectangular domain $\Omega = \{(x, y) | x \in (0, L_x), y \in (0, L_y)\}$. In terms of the stream function ψ , the governing equation is

$$\frac{\partial}{\partial t} \left(\Delta\psi - \frac{1}{R_d^2} \psi \right) + J(\psi, \Delta\psi) + \beta_0 \frac{\partial\psi}{\partial x} = \nu \Delta^2 \psi + F(x), \quad (2.1)$$

where $R_d = \frac{\sqrt{g'H_1}}{f_0}$ is the deformation radius, g' is the reduced gravity constant, H_1 is the depth of the west boundary layer, ν is the eddy viscosity coefficient, f_0 is the constant Coriolis parameter, β_0 is the derivative of the Coriolis parameter, $F(x)$ is the force in relation to wind stress (curl of the wind stress) acting on the sea surface, and $J(u, v) := \frac{\partial u}{\partial x} \frac{\partial v}{\partial y} - \frac{\partial u}{\partial y} \frac{\partial v}{\partial x}$. Periodic boundary condition is assumed in the y -direction, and the no-slip no-penetration boundary condition is prescribed in the x -direction:

$$\psi(0, y) = \psi(a, y) = \frac{\partial\psi(0, y)}{\partial x} = \frac{\partial\psi(a, y)}{\partial x} = 0. \quad (2.2)$$

The term $\Delta\psi - \frac{1}{R_d^2} \psi$ is recognized as the potential vorticity. Note that the term $\frac{1}{R_d^2} \psi$ in the potential vorticity disappears in the Jacobian J due to the skew-symmetry of J . The EB model can be viewed as a simplification of the more often used two-layer model when the lower layer is at rest. It can be derived as a quasi-geostrophic approximation of the shallow water equation in the two-layer setting. We refer to [3, 19, 22, 27] for the detailed derivation of the EB model.

The wind force $F(x)$ is uniform in the y -direction which determines a steady-state (meridional flow) of the form $\Psi_s(x) = \Psi_0 \psi_s(x)$ with Ψ_0 being the characteristic value of

the steady-state stream function. In light of the definition of $J(\cdot, \cdot)$, one infers that the steady-state stream function $\psi_s(x)$ satisfies the following ordinary differential equation

$$-v \frac{d^4 \psi_s}{dx^4} + \beta_0 \frac{d\psi_s}{dx} = \frac{F(x)}{\Psi_0}$$

supplemented with the same boundary conditions as (2.2). In this study we shall adopt the celebrated Munk boundary layer profile (specified below) for the steady-state flow following [3, 11, 20].

For notational simplicity, let us denote the perturbation around $\Psi_s(x)$ also by ψ , and insert $\Psi_s(x) + \psi$ into the system (2.1)

$$\begin{aligned} \frac{\partial}{\partial t} \left(\Delta\psi - \frac{1}{R_d^2} \psi \right) + J(\psi, \Delta\psi) + \beta_0 \frac{\partial \psi}{\partial x} \\ = v \Delta^2 \psi - J(\Psi_s, \Delta\psi) - J(\psi, \Delta\Psi_s). \end{aligned} \quad (2.3)$$

As is appropriate for the study of western boundary layer, cf. [3], we choose the viscous boundary layer length scale $\delta_M = \left(\frac{v}{\beta_0}\right)^{\frac{1}{3}}$ to be the length scale; $\frac{\Psi_0}{\delta_M}$ to be the velocity scale which gives the time scale $\frac{\delta_M^2}{\Psi_0}$. The nondimensionalization of Eq. (2.3) gives

$$\frac{\partial}{\partial t} (\Delta\psi - S\psi) + u_s \frac{\partial \Delta\psi}{\partial y} - \frac{\partial \psi}{\partial y} \frac{d^2 u_s}{dx^2} + J(\psi, \Delta\psi) + \frac{1}{R} \frac{\partial \psi}{\partial x} = \frac{1}{R} \Delta^2 \psi. \quad (2.4)$$

Here $R = \frac{\Psi_0}{v}$ is the Reynolds number, $S = \left(\frac{\delta_M}{R_d}\right)^2$ is the square of the ratio of the Munk scale to the Rossby deformation radius which can be viewed as a measure of stratification in the EB model as well. The case $S \rightarrow 0$ gives rise to the barotropic QG equation, cf. [19, 22]. In this work, we limit our study to viscous instability of the western boundary currents represented by the Munk profile, cf. [11], i.e.,

$$u_s = \frac{d\psi_s}{dx} = e^{-\frac{x}{2}} \sin \frac{\sqrt{3}}{2} x. \quad (2.5)$$

Note that the Munk-profile satisfies the steady-state equation with zero forcing $F = 0$ (constant wind stress). We remark that the real western boundary current is due to nonzero F which would give a different boundary layer profile. The Munk-profile is an approximation and convenient for theoretical analysis. It will be clear that our method applies to general boundary layer profile.

Throughout the remainder of this article, we use parameters a and b to represent the dimensionless length in the x and y directions respectively. We introduce the aspect ratio $\alpha = \frac{b}{a}$. In the following sections, we study the instability and transition of the Munk boundary layer profile based on the perturbation Eq. (2.4) as R, S, α vary.

3 The eigenvalue problem and principle of exchange of stability

The Munk boundary layer profile introduced in (2.5) is of shear flow type which tends to be unstable at large Reynolds number [1,3,11]. In what follows we will study the instabilities of the Munk profile and the resulting transitions to new states from the perspective of the dynamic transition theory developed by Ma and Wang [18]. We first establish the so-called Principle of Exchange of Stability (PES) from a linear stability analysis, cf. Assumption 3.1, determining the critical Reynolds number at which the basic profile loses stability. We then reduce the original system of partial differential equations to a system of ordinary differential equations on the center manifold generated by the unstable modes at the critical Reynolds number. The dynamic transition is studied via the reduced system.

We proceed with the linear stability analysis. Let us consider the linear part of Eq. (2.4), i.e., without the nonlinear term $J(\psi, \Delta\psi)$. Since periodic boundary condition is prescribed in the y -direction and the coefficients of the linear equation depend only on x , the following separation of variables (normal mode ansatz) can be assumed

$$\psi = e^{ib_m y + \beta t} u(x), \quad b_m = 2m\pi/b, \quad m \in \mathbb{Z}, \quad \beta \in \mathbb{C},$$

which leads to an eigenvalue problem similar to the celebrated Orr-Sommerfeld equation [9]

$$\begin{aligned} (D^2 - b_m^2)^2 u - iRb_m u_s (D^2 - b_m^2) u + iRb_m u_s'' u - Du \\ = \beta R (D^2 - b_m^2 - S) u, \\ u(0) = Du(0) = u(a) = Du(a) = 0. \end{aligned} \quad (3.1)$$

Here we adopt the notation D for the derivative with respect to x , i.e., $D = \frac{d}{dx}$. It is clear that the eigenvalues β are discrete. Note also that the eigenvalues and eigenfunctions corresponding to $-m$ are the complex conjugate of the respective eigenvalues and eigenfunctions corresponding to m . Hence we only need to consider nonnegative m 's. For the sake of convenience, let us define a family of ordinary differential operators \mathcal{A}_m and \mathcal{L}_m as follows

$$\begin{aligned} \mathcal{A}_m u &= R(D^2 - b_m^2 - S)u, \quad m = 0, 1, 2, \dots, \\ \mathcal{L}_m u &= (D^2 - b_m^2)^2 u - iRb_m u_s (D^2 - b_m^2) u + iRb_m u_s'' u - Du. \end{aligned} \quad (3.2)$$

Then, the eigenvalue problem can be expressed in an abstract form

$$\mathcal{L}_m u_k = \beta_k \mathcal{A}_m u_k, \quad k = 1, 2, \dots \rightarrow \infty, \quad \forall m \in \mathbb{Z}_0^+. \quad (3.3)$$

We also need the adjoint eigenvalue problem

$$\mathcal{L}_m^* u_k^* = \beta_k \mathcal{A}_m^* u_k^*, \quad k = 1, 2, \dots \rightarrow \infty, \quad \forall m \in \mathbb{Z}_0^+, \quad (3.4)$$

where the dual operator \mathcal{L}_m^* is defined by

$$(\mathcal{L}_m u, v) = (u, \mathcal{L}_m^* v).$$

It is evident that the eigenvalue problem (3.1) can not be solved explicitly, as in the case of Orr-Sommerfeld equation. In Section 4, we will describe a spectral method for numerically solving the eigenvalue problem. Nonetheless, by a simple energy argument we can show that modes of large wave number (b_m large) tend to be stable for fixed Reynolds number, and that there exists a Reynolds number below which all modes are stable. Similar results also hold for Orr-Sommerfeld equation, cf. [9]. More precisely, we have the following proposition:

Proposition 3.1. For the eigenvalue problem (3.3), the zero mode $m = 0$ is always stable. Moreover, there exists a positive number $C = \frac{R\|u_s\|_\infty}{2}$ such that for all $b_m \geq C$, the corresponding eigenvalues from (3.3) have negative real part, i.e. $Re(\beta_k) < 0$. In particular, if $R \leq \frac{4\pi}{b\|u_s\|_\infty}$, then the basic profile ψ_s is stable.

Proof. For notational simplicity we omit the dependence of variables on the index k . Using \bar{u} to express the conjugate of u , $\langle \cdot, \cdot \rangle$ and $\| \cdot \|$ to express the complex $L^2(0, a)$ - inner product and norm respectively, then taking the L^2 inner product of (3.1) with \bar{u} one derives that

$$Re(\beta) = \frac{D_1 - D_2}{D_3}, \tag{3.5}$$

in which D_i ($i = 1, 2, 3$) are

$$\begin{aligned} D_1 &= Re(iRb_m \langle u_s D^2 u, u \rangle) + Re(\langle Du, u \rangle), \\ D_2 &= \langle D^2 u, D^2 u \rangle + 2b_m^2 \langle Du, Du \rangle + b_m^4 \langle u, u \rangle, \\ D_3 &= R(\langle Du, Du \rangle) + R(b_m^2 + S) \langle u, u \rangle. \end{aligned}$$

Here R is the Reynolds number, $Im(A)$ represents the imaginary part of A , and $Re(A)$ is the real part of A , where A is a function of complex value. It is clear that $D_1 - D_2 < 0$ would imply $Re(\beta) < 0$. Since

$$\begin{aligned} Re(\langle Du, u \rangle) &= \frac{1}{2} (\langle Du, u \rangle + \langle u, Du \rangle) \\ &= \frac{1}{2} \int_0^a \frac{d(|u|^2)}{dz} dz = 0, \end{aligned}$$

it follows that

$$D_1 \leq \frac{Rb_m \|u_s\|_\infty}{2C_1} \langle D^2 u, D^2 \bar{u} \rangle + \frac{Rb_m C_1 \|u_s\|_\infty}{2} \langle u, \bar{u} \rangle.$$

Hence

$$D_1 - D_2 \leq \left(\frac{Rb_m \|u_s\|_\infty}{2C_1} - 1 \right) \langle D^2 u, D^2 \bar{u} \rangle - 2b_m^2 \langle Du, D\bar{u} \rangle \\ + \left(\frac{Rb_m C_1 \|u_s\|_\infty}{2} - b_m^4 \right) \langle u, \bar{u} \rangle.$$

It is clear that $D_1 - D_2 < 0$ when $m=0$ ($b_m=0$). That is the mode $m=0$ is stable. Otherwise, for $m \neq 0$, let $C_1 = \frac{Rb_m \|u_s\|_\infty}{2}$. Then

$$\frac{Rb_m C_1 \|u_s\|_\infty}{2} - b_m^4 \leq 0 \Rightarrow \operatorname{Re}(\beta) < 0.$$

It follows that there exists a positive number $C = \frac{R \|u_s\|_\infty}{2}$ such that for all $b_m \geq C$, the corresponding eigenvalues have negative real part. Furthermore, it is clear that

$$R \leq \min_{m \in \mathbb{Z}^+} \frac{2b_m}{\|u_s\|_\infty} = \frac{4\pi}{b \|u_s\|_\infty} \Rightarrow \operatorname{Re}(\beta) < 0.$$

This concludes the proof of the proposition. \square

Remark 3.1. The bound derived here is by no means optimal. Better bounds can be obtained following [25].

Proposition 3.1 suggests the existence of a critical Reynolds number, possibly depending on the stratification S and the aspect ratio α , across which certain modes will lose stability. For the development of the nonlinear instability and transition theory, we need the PES condition. Without loss of generality we assume that the eigenvalues $\{\beta_{m,k}\}_{m,k}$ of L_m are ordered by decreasing real part for each m . That is, we assume that

$$\operatorname{Re} \beta_{m,1} \geq \operatorname{Re} \beta_{m,2} \geq \dots \rightarrow -\infty, \quad \forall m \in \mathbb{Z}^+.$$

Then the principle of exchange of stabilities (PES condition) takes the following form:

Assumption 3.1 (Principle of Exchange of Stabilities). There exists an integer $n \in \mathbb{Z}^+$ and a critical Reynolds number $R^* > 0$ such that, for a small $\delta > 0$ the eigenvalues satisfy

$$\operatorname{Re} \beta_{n,1}(R) \begin{cases} > 0 & \text{if } R^* < R < R^* + \delta, \\ = 0 & \text{if } R = R^*, \\ < 0 & \text{if } R < R^*, \end{cases} \quad (3.6)$$

$$\operatorname{Re} \beta_{m,k}(R^*) < 0 \quad \text{if } m \neq n \text{ or } k > 1. \quad (3.7)$$

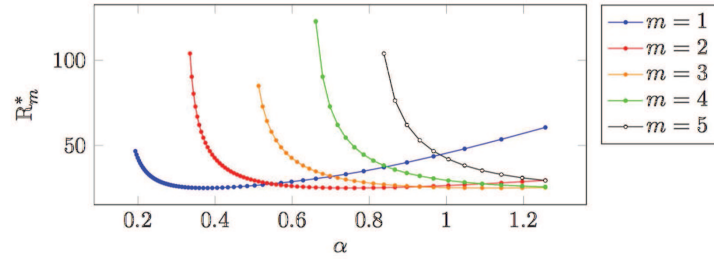


Figure 1: The mode-dependent critical Reynolds number, i.e. zero of $\text{Re}\beta_{m,1}(R_m^*)=0$ as a function of the aspect ratio $\alpha = \frac{b}{a}$ with $a=50$ fixed for different m .

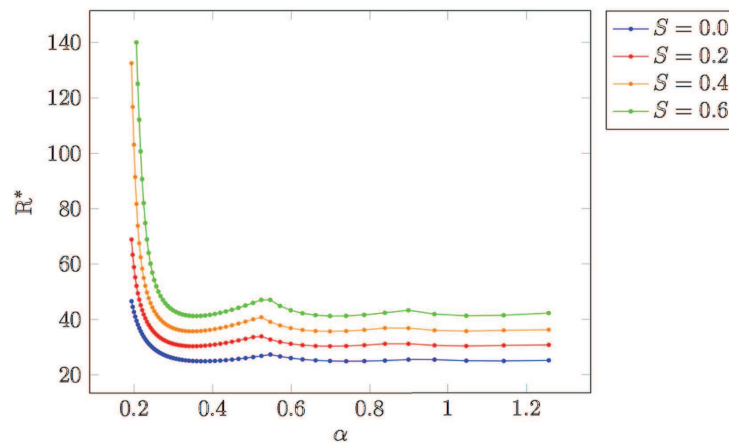


Figure 2: Neutral curves, $R^* = \min_{m \in \mathbb{N}} R_m^*$ in which $\text{Re}\beta_{m,1}(R_m^*)=0$ for different aspect ratio $\alpha = b/a$, where a is taken as 50.

It is generally a challenge to verify the PES condition rigorously, except when the eigenvalue problem can be solved analytically. Here we resort to numerical solutions of the eigenvalue problem and establish the PES condition numerically. We explore the values of the critical R^* from a global perspective. More precisely, we compute for each $\alpha > 0$ the value R_m^* such that $\text{Re}\beta_{m,1}=0$. By doing this we obtain, for each m , a curve $R_m^* = R_m^*(\alpha)$ that determines the onset of linear instability. Plots of mode-dependent critical Reynolds number $R_m^*(\alpha)$ as a function of α are shown in Fig. 1 for a few selected values of m .

Furthermore, for all but countably many values of α , there is only one wavenumber $n = n(\alpha)$ for which $R_n^* = \min_{m \in \mathbb{N}} R_m^*$. Thus this is the value $R^* = R_n^*$ at which the first transition occurs. This defines a continuous function $R^* = R^*(\alpha)$ that is piecewise smooth, with possible cusp points or corners at the values of α for which there is more than one wavenumber n giving rise to linear instability. The neutral curves $R^*(\alpha)$ is shown in Fig. 2 for different stratification S . Here, it is worth mentioning that $\text{Im}\beta_{n,1} \neq 0$ for all

parameters $S \in [0.1, 0.9]$ and $\alpha \in [0.1, 1.3]$, where $\alpha = b/a$ is the aspect ratio.

We will proceed under the working assumption that the integer n has been chosen to satisfy the PES condition. As soon as linear instabilities occur at the critical Reynolds number, the nonlinear system (2.4) undergoes a dynamic transition classified as one of the three types: continuous, catastrophic, or random, cf. [18]. In the following we study the transition as R crosses the critical value R^* , for different values of S and α .

4 The transition theory

Following the dynamic transition theory [18], the type of transitions is determined by reducing the nonlinear system (2.4) to the center manifold in the first unstable eigenmodes. Specifically one can establish that:

Lemma 4.1. *The transition of the nonlinear system (2.4) at $R = R^*$ is equivalent to that of the following ordinary differential equation*

$$\frac{d\eta}{dt} = \beta_{n,1}\eta + P\eta|\eta|^2 + o(|\eta|^3), \quad (4.1)$$

where η is complex-valued, and P is the transition number whose sign determines the transition types.

Proof. The rigorous theory of the equivalence can be found in [18]. Here we focus on deriving the reduced equation (4.1) with particular emphasis on the expression of the transition number P . Denote the central space by H_c which is the span of the eigenfunctions corresponding to $\beta_{n,1}$. Denote the first eigenfunction and its dual (the real part of corresponding eigenvalue changes its sign at $R = R^*$) as follows

$$\varphi_1 = e^{ib_n y} u_1(x), \quad \varphi_1^* = e^{ib_n y} u_1^*(x). \quad (4.2)$$

Any element ϕ in H_c can be expressed as

$$\phi = \eta \varphi_1 + \overline{\eta} \overline{\varphi_1}. \quad (4.3)$$

This is an important observation and simplifies our calculation later. Following the abstract approximate expression of the central manifold given by (A.2.14) in [18], we assume the central manifold function $h(\phi)$ takes the following form

$$h(\phi) = h_2(\phi) + o(|\eta|^2),$$

where $h_2(\phi)$ is the quadratic part of the center manifold function. Then, straightforward calculation shows that h_2 needs to satisfy

$$\begin{aligned} 2\beta_1 A h_2(\phi) - \mathcal{L} h_2(\phi) &= \mathcal{G}(\phi, \phi) \\ &= \eta^2 \mathcal{G}(\varphi_1, \varphi_1) + \overline{\eta}^2 \mathcal{G}(\overline{\varphi_1}, \overline{\varphi_1}) + |\eta|^2 (\mathcal{G}(\varphi_1, \overline{\varphi_1}) + \mathcal{G}(\overline{\varphi_1}, \varphi_1)). \end{aligned} \quad (4.4)$$

where $\mathcal{G}(a,b)$ is defined by

$$\mathcal{G}(a,b) = J(a,\Delta b), \tag{4.5}$$

and the linear differential operators \mathcal{A} and \mathcal{L} are defined as

$$\mathcal{A}\psi = \Delta\psi - S\psi, \quad \mathcal{L}\psi = \frac{1}{Re} \Delta^2\psi - u_s \frac{\Delta\psi}{\partial y} + \frac{\partial\psi}{\partial y} \frac{d^2u_s}{dx^2} - \frac{1}{Re} \frac{\partial\psi}{\partial x}. \tag{4.6}$$

In view of definition (4.2) one calculates

$$\begin{aligned} \mathcal{G}(\varphi_1, \varphi_1) &= ib_n e^{ib_{2n}y} (u_1 u_1''' - u_1' u_1''), \\ \mathcal{G}(\overline{\varphi_1}, \overline{\varphi_1}) &= -ib_n e^{-ib_{2n}y} (\overline{u_1 u_1''' - u_1' u_1''}), \\ \mathcal{G}(\varphi_1, \overline{\varphi_1}) &= ib_n (u_1 \overline{u_1}''' + u_1' \overline{u_1}'' - b_n^2 u_1' \overline{u_1} - b_n^2 u_1 \overline{u_1}'), \\ \mathcal{G}(\overline{\varphi_1}, \varphi_1) &= -ib_n (\overline{u_1} u_1''' + \overline{u_1}' u_1'' - b_n^2 \overline{u_1}' u_1 - b_n^2 \overline{u_1} u_1'). \end{aligned} \tag{4.7}$$

Hence

$$\mathcal{G}(\varphi_1, \overline{\varphi_1}) + \mathcal{G}(\overline{\varphi_1}, \varphi_1) = ib_n (u_1 \overline{u_1}''' + u_1' \overline{u_1}'' - \overline{u_1} u_1''' + \overline{u_1}' u_1''). \tag{4.8}$$

Let $h_2(\phi)$ be

$$h_2(\phi) = \eta^2 \phi_{20} + |\eta|^2 \phi_{11} + \overline{\eta}^2 \phi_{02} + o(|\eta|^2), \tag{4.9}$$

where $\phi_{20}, \phi_{11}, \phi_{02}$ have the following ansatz

$$\begin{aligned} \phi_{20} &= e^{ib_{2n}y} M_1(x), \\ \phi_{11} &= M_2(x), \\ \phi_{02} &= -e^{-ib_{2n}y} M_3(x). \end{aligned} \tag{4.10}$$

Eq. (4.4) implies that M_i ($i=1,2,3$) should satisfy

$$\begin{aligned} 2\beta_{n,1} \mathcal{A}_{2n} M_1 - \mathcal{L}_{2n} M_1 &= e^{-i2b_n y} \mathcal{G}(\varphi_1, \varphi_1), \\ 2\overline{\beta_{n,1}} \mathcal{A}_{2n} M_3 - \mathcal{L}_{2n} M_3 &= e^{i2b_n y} \mathcal{G}(\overline{\varphi_1}, \overline{\varphi_1}), \\ 2\text{Re}(\beta_{n,1}) \mathcal{A}_0 M_2 - \mathcal{L}_0 M_2 &= \mathcal{G}(\varphi_1, \overline{\varphi_1}) + \mathcal{G}(\overline{\varphi_1}, \varphi_1), \end{aligned} \tag{4.11}$$

where one may refer to Eqs. (3.2) for the definition of \mathcal{A}_{2n} and \mathcal{L}_{2n} . On the other hand, one observes from (4.7) that

$$\phi_{20} = \overline{\phi_{02}}.$$

Hence, one only needs to solve

$$\begin{aligned} 2\beta_{n,1} \mathcal{A}_{2n} M_1 - \mathcal{L}_{2n} M_1 &= e^{-i2b_n y} \mathcal{G}(\varphi_1, \varphi_1), \\ 2\text{Re}(\beta_{n,1}) \mathcal{A}_0 M_2 - \mathcal{L}_0 M_2 &= \mathcal{G}(\varphi_1, \overline{\varphi_1}) + \mathcal{G}(\overline{\varphi_1}, \varphi_1), \\ M_1(0) = M_1'(a) = M_2(0) = M_2'(a) &= 0. \end{aligned} \tag{4.12}$$

Applying the general formula of the reduced equation (A.2.12) in [18], one derives the reduced equation

$$\frac{d\eta}{dt} = \beta_{n,1}\eta + (\mathcal{G}(\varphi, \varphi) + \mathcal{G}(\varphi, h_2) + \mathcal{G}(h_2, \varphi), \varphi_1^*) + o(|\eta|^3), \quad (4.13)$$

in which φ_1 and φ_1^* are chosen to satisfy the normalizing condition:

$$(\Delta\varphi_1, \varphi_1^*)/b = \frac{1}{b} \int_0^a \int_0^b \Delta\varphi_1 \overline{\varphi_1^*} dx dz = 1.$$

It follows from (4.3) and (4.9) that

$$\begin{aligned} (\mathcal{G}(\varphi, h_2), \varphi_1^*) &= (\mathcal{G}(\eta\varphi_1 + \overline{\eta\varphi_1}, \eta^2\phi_{20} + |\eta|^2\phi_{11} + \overline{\eta^2}\phi_{02}), \varphi_1^*) \\ &= \eta^3(\mathcal{G}(\varphi_1, \phi_{20}), \varphi_1^*) + \eta|\eta|^2(\mathcal{G}(\overline{\varphi_1}, \phi_{20}), \varphi_1^*) \\ &\quad + \eta|\eta|^2(\mathcal{G}(\varphi_1, \phi_{11}), \varphi_1^*) + \overline{\eta}|\eta|^2(\mathcal{G}(\overline{\varphi_1}, \phi_{11}), \varphi_1^*) \\ &\quad + \overline{\eta}|\eta|^2(\mathcal{G}(\varphi_1, \phi_{02}), \varphi_1^*) + \overline{\eta}^3(\mathcal{G}(\overline{\varphi_1}, \phi_{02}), \varphi_1^*), \end{aligned} \quad (4.14)$$

$$\begin{aligned} (\mathcal{G}(h_2, \varphi), \varphi_1^*) &= (\mathcal{G}(\eta^2\phi_{20} + |\eta|^2\phi_{11} + \overline{\eta^2}\phi_{02}, \eta\varphi_1 + \overline{\eta\varphi_1}), \varphi_1^*) \\ &= \eta^3(\mathcal{G}(\phi_{20}, \varphi_1), \varphi_1^*) + \eta|\eta|^2(\mathcal{G}(\phi_{20}, \overline{\varphi_1}), \varphi_1^*) \\ &\quad + \eta|\eta|^2(\mathcal{G}(\phi_{11}, \varphi_1), \varphi_1^*) + \overline{\eta}|\eta|^2(\mathcal{G}(\phi_{11}, \overline{\varphi_1}), \varphi_1^*) \\ &\quad + \overline{\eta}|\eta|^2(\mathcal{G}(\phi_{02}, \varphi_1), \varphi_1^*) + \overline{\eta}^3(\mathcal{G}(\phi_{02}, \overline{\varphi_1}), \varphi_1^*), \end{aligned} \quad (4.15)$$

Using (4.2) and (4.10) one finds that

$$\begin{aligned} (\mathcal{G}(\varphi_1, \phi_{20}), \varphi_1^*) &= (\mathcal{G}(\phi_{20}, \varphi_1), \varphi_1^*) = 0, \\ (\mathcal{G}(\overline{\varphi_1}, \phi_{11}), \varphi_1^*) &= (\mathcal{G}(\phi_{11}, \overline{\varphi_1}), \varphi_1^*) = 0, \\ (\mathcal{G}(\varphi_1, \phi_{02}), \varphi_1^*) &= (\mathcal{G}(\phi_{02}, \varphi_1), \varphi_1^*) = 0, \\ (\mathcal{G}(\overline{\varphi_1}, \phi_{02}), \varphi_1^*) &= (\mathcal{G}(\phi_{02}, \overline{\varphi_1}), \varphi_1^*) = 0. \end{aligned}$$

It follows that

$$\begin{aligned} &(\mathcal{G}(\varphi, h_2), \varphi_1^*) + (\mathcal{G}(h_2, \varphi), \varphi_1^*) \\ &= ((\mathcal{G}(\overline{\varphi_1}, \phi_{20}), \varphi_1^*) + (\mathcal{G}(\varphi_1, \phi_{11}), \varphi_1^*) + (\mathcal{G}(\phi_{20}, \overline{\varphi_1}), \varphi_1^*) + (\mathcal{G}(\phi_{11}, \varphi_1), \varphi_1^*))\eta|\eta|^2. \end{aligned} \quad (4.16)$$

Therefore, the reduced equation (4.13) is simplified as

$$\frac{d\eta}{dt} = \beta_{n,1}\eta + P\eta|\eta|^2 + o(|\eta|^3).$$

where P is given by the following integral

$$\begin{aligned} P &= (\mathcal{G}(\overline{\varphi_1}, \phi_{20}), \varphi_1^*) + (\mathcal{G}(\varphi_1, \phi_{11}), \varphi_1^*) \\ &\quad + (\mathcal{G}(\phi_{20}, \overline{\varphi_1}), \varphi_1^*) + (\mathcal{G}(\phi_{11}, \varphi_1), \varphi_1^*). \end{aligned} \quad (4.17)$$

Indeed, the exact expression of the transition number P can be written as follows

$$\begin{aligned}
 P = & 4ni\pi \int_0^a \overline{u_1} u_1^* (M_1'' - 4b_n^2 M_1) dx + 2ni\pi \int_0^a \overline{u_1} u_1^* (M_1''' - 4b_n^2 M_1') dx \\
 & - 2ni\pi \int_0^a M_1' \overline{u_1} u_1^* (u_1'' - b_n^2 u_1) dx - 4ni\pi \int_0^a M_1 \overline{u_1} u_1^* (u_1''' - b_n^2 u_1') dx \\
 & - 2ni\pi \int_0^a u_1 \overline{u_1} M_2''' dx + 2ni\pi \int_0^a M_2' \overline{u_1} u_1^* (u_1'' - b_n^2 u_1) dx.
 \end{aligned}$$

This completes the proof. □

Now we are ready to state the main transition theorem.

Theorem 4.1. *If the first simple eigenvalue is complex, then the following two assertions hold true:*

- (1) *If $\text{Re}P = P_1 < 0$, the system (2.4) undergoes a continuous transition (a supercritical Hopf bifurcation) at $R=R^*$. In particular, the steady-state solution 0 bifurcates to a stable periodic trajectory Γ at $R=R^*$, satisfying $\Gamma \rightarrow 0$, as $R \rightarrow R^{*+}$. Furthermore, the periodic orbit can be approximated by the following formula*

$$\varphi = \left(\frac{\beta_{11}}{|P_1|} \right)^{\frac{1}{2}} \left(e^{i\beta_{12}t} \varphi_1 + e^{-i\beta_{12}t} \overline{\varphi_1} \right) + o\left(|\beta_{11}|^{\frac{1}{2}}\right), \tag{4.18}$$

where $\beta_{11} > 0, \beta_{n,1} = \beta_{11} + i\beta_{12}$ and $\varphi_1 = e^{ib_n y} u_1(x)$ with $u_1(x)$ the corresponding eigenfunction. The topological structure of the continuous transition is illustrated in Fig. 3.

- (2) *If $\text{Re}P = P_1 > 0$, the system (2.4) undergoes a catastrophic transition (subcritical Hopf bifurcation) at $R=R^*$. An unstable periodic orbit Γ_1 collides with the steady-state 0 leading to the loss of stability of 0 at the critical number R^* . In addition, there exists a subcritical number R_s ($R_s \leq R^*$) at which there exists a singular separation of periodic orbits, and a nonzero attractor Γ_2 bifurcates from 0 at $R=R_s$. In particular, there is no periodic solution bifurcating from 0 for $R > R^*$. The topological structure of the catastrophic transition is illustrated in Fig. 4.*

Remark 4.1. We can deduce from Theorem 4.1 that, there exist two types of transition-continuous and catastrophic transitions for system (2.4) at $R=R^*$. For continuous one, the flow will become from Munk profile to a periodic motion while for catastrophic one the flow jumps to another state which in general belongs to an attractor containing more than one asymptotic state, cf. Fig. 4.

Proof. It is known that the reduced equation is

$$\frac{d\eta}{dt} = \beta_{n,1}\eta + P\eta|\eta|^2 + o(|\eta|^3)$$

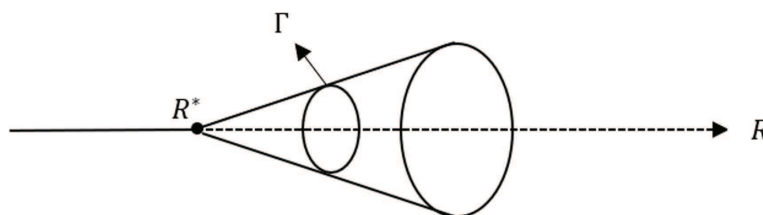


Figure 3: Topological structure of the continuous transition $ReP < 0$. A Hopf bifurcation occurs at R^* , indicating that a stable limit cycle Γ bifurcates from 0 at $R = R^*$, and whose size grows continuously with R .

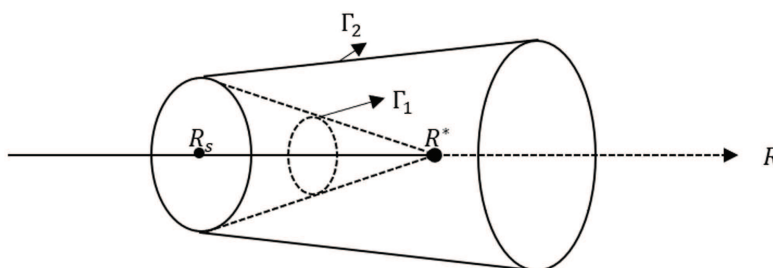


Figure 4: Topological structure of the catastrophic transition $ReP > 0$. A periodic orbit Γ_1 occurs from 0 on $R < R^*$. A nonzero attractor Γ_2 appears at R_s .

from which we have

$$\frac{d\bar{\eta}}{dt} = \overline{\beta_{n,1}}\bar{\eta} + \bar{P}\bar{\eta}|\eta|^2 + o(|\eta|^3).$$

Straightforward calculation gives

$$\begin{aligned} \left. \frac{d|\eta|^2}{dt} \right|_{R=R^*} &= \eta \left. \frac{d\bar{\eta}}{dt} \right|_{R=R^*} + \bar{\eta} \left. \frac{d\eta}{dt} \right|_{R=R^*} \\ &= \left(2\text{Re}(\beta_{n,1})|\eta|^2 + \text{Re}(P)|\eta|^4 + o(|\eta|^4) \right) \Big|_{R=R^*} \\ &= P_1|\eta|^4 + o(|\eta|^4). \end{aligned} \tag{4.19}$$

Then, (4.19) means that 0 is local global stable point of (2.4) at $R = R^*$ if $P_1 < 0$. Therefore, using Theorem 2.3.5 in [18], (2.4) bifurcates from $(\psi, R) = (0, R^*)$ to a stable periodic solution on $R > R^*$. Similarly, if $P_1 > 0$, it is clear that 0 is unstable, (2.4) bifurcates from $(\psi, R) = (0, R^*)$ to an unstable periodic solution on $R < R^*$. Using Theorem 2.5.4 in [18], there exists a subcritical number $R = R_s$ at which (2.4) has a singular separation of periodic orbits. \square

Remark 4.2. Theorem 4.1 does not cover the case $ReP = 0$. In the case of $ReP = 0$, higher order approximation of the center manifold function (e.g. third order part of the center

manifold function) is needed in Lemma 4.1. Similar transition theorem can be established, albeit with more involved calculation.

5 Numerical evaluation and results

Theorem 4.1 says that the types of the transition of the nonlinear system (2.4) are completely determined by the sign of the transition number P defined in (4.17). To numerically evaluate the transition number, one needs to find the critical Reynolds number, solve for the first eigenfunction and its dual from Eqs. (3.3) and (3.4) respectively, and then evaluate P using (4.17). In what follows we first introduce a Legendre-spectral method for solving Eqs. (3.3) and (3.4), and present the steps for computing transition number P . Then we demonstrate the numerical results and the physical implications. See [26] for a comprehensive study of the spectral method.

5.1 Numerical procedures for the evaluation of P

Let us define a function space H_1 as follows:

$$H_1 = \{u \in H^2(-1,1) \mid u(-1) = u(1) = u'(-1) = u'(1) = 0\}. \quad (5.1)$$

It is clear that the eigenfunction u_k in (3.3) belongs to H_1 . Now we approximate H_1 by the following finite dimension subspace, cf. [26]

$$\begin{aligned} H_{1,N} &= \{\sum_{m=0}^{N-4} c_m \omega_m \mid c_m \in \mathbb{R}\}, \quad N = 6, 7, \dots, \\ \omega_m &= d_m \left(L_m - \frac{2(2m+5)}{2m+7} L_{m+2} + \frac{2m+3}{2m+7} L_{m+4} \right), \\ d_m &= \frac{1}{\sqrt{2(2m+3)^2(2m+5)}}, \\ \{L_m\}_{m=0}^{\infty} &\text{ is a family of Legendre orthogonal polynomials.} \end{aligned}$$

Now let u^N be given by

$$u^N = \sum_{m=0}^{N-4} p_m \omega_m.$$

Let L^n and A^n be the matrices with elements given by respectively

$$\begin{aligned} L_{ij}^n &= (\mathcal{L}_n(\omega_i), \omega_j), \\ A_{ij}^n &= (\mathcal{A}_n(\omega_i), \omega_j). \end{aligned} \quad (5.2)$$

We refer to (4.6) for the definition of \mathcal{L} and \mathcal{A} . Then Eq. (3.2) gives

$$L^n = \sum_{i=1}^6 C_i, \quad A^n = D_1 + D_2, \quad (5.3)$$

in which C_i ($i=1, \dots, 6$) and D_i ($i=1, 2$) are given by

$$\begin{aligned} C_1 &= (D^2\omega_i, D^2\omega_j), & C_2 &= 2b_n^2(D\omega_i, D\omega_j), \\ C_3 &= (b_n^4 + i\text{Re}b_n^3)(\omega_i, \omega_j), & C_4 &= (\omega_i, D\omega_j), \\ C_5 &= -i\text{Re}b_n(u_s D^2\omega_i, \omega_j), & C_6 &= i\text{Re}b_n(u_s''\omega_i, \omega_j), \\ D_1 &= -\text{Re}(D\omega_i, D\omega_j), & D_2 &= -\text{Re}(b_n^2 + S)(\omega_i, \omega_j). \end{aligned} \quad (5.4)$$

Then, it follows from Eq. (3.3) that

$$(A^n)^{-1} L^n P_N^{n,k} = \lambda_{n,k} P_N^{n,k}, \quad (5.5)$$

in which $P_N^{n,k}$ is defined as

$$P_N^{n,k} = \begin{pmatrix} p_0^{n,k} \\ \vdots \\ p_{N-4}^{n,k} \end{pmatrix}, \quad (5.6)$$

$$\text{Re}\lambda_{n,1} \geq \text{Re}\lambda_{n,2} \geq \text{Re}\lambda_{n,3} \cdots. \quad (5.7)$$

It is clear that the first eigenvalue is numerically given by

$$\text{Re}\beta_{n,1} = \text{Re}\lambda_{n,1} = \min_{m \in \mathbb{N}} \text{Re}\lambda_{m,1}. \quad (5.8)$$

And the critical Reynolds number R^* is then determined by solving equation

$$\text{Re}\lambda_{n,1}(R) = 0. \quad (5.9)$$

For different stratification number S and aspect ratio α , the solutions of (5.9) are shown in Fig. 2.

Now the evaluation of the transition number P can be decomposed into several steps as follows:

1. Solving the linear equation (5.5), one can get the approximate first eigenfunction $\phi_1^N = \sum_{i=0}^{N-4} p_i^{n,1} \omega_i$ and its dual $\phi_1^{*N} = \sum_{i=0}^{N-4} p_i^{n,1} \omega_i$, which satisfy $(\mathcal{A}\phi_1^N, \phi_1^{*N}) = 1$.
2. Using the results obtained from the first step one can compute

$$\begin{aligned} \phi_1^N (\phi_1^N)''' - (\phi_1^N)' (\phi_1^N)'' &= \sum_{i=0}^{N-4} M_i^{1N} \omega_i, \\ \phi_1^N (\overline{\phi_1^N})''' + (\phi_1^N)' (\overline{\phi_1^N})'' - \overline{\phi_1^N} (\phi_1^N)''' + (\overline{\phi_1^N})' (\phi_1^N)'' &= \sum_{i=0}^{N-4} M_i^{2N} \omega_i. \end{aligned}$$

3. Based on the results in the second step, one computes

$$S_{i1}^N = \sum_{j=0}^{N-4} \left((L^{2m^*})^{-1} \right)_{ij} M_j^{1N}, \quad S_{i2}^N = \sum_{j=0}^{N-4} \left((L^0)^{-1} \right)_{ij} M_j^{2N}.$$

4. Let ϕ_{20}^N and ϕ_{11}^N be given by

$$\begin{aligned}\phi_{20}^N &= ib_{m^*} e^{ib_{m^*} y} \sum_{i=0}^{N-4} S_{i1}^N \omega_i, \\ \phi_{11}^N &= ib_{m^*} \sum_{i=0}^{N-4} S_{i2}^N \omega_i, \\ \varphi_1^N &= e^{ib_n y} \phi_1^N, \quad \varphi_1^{*N} = e^{ib_n y} \phi_1^{*N},\end{aligned}$$

then the transition number P is evaluated by

$$\begin{aligned}P &= \left(\mathcal{G}(\overline{\varphi_1^N}, \phi_{20}^N), \varphi_1^{*N} \right) + \left(\mathcal{G}(\varphi_1^N, \phi_{11}^N), \varphi_1^{*N} \right) \\ &\quad + \left(\mathcal{G}(\phi_{20}^N, \overline{\varphi_1^N}), \varphi_1^{*N} \right) + \left(\mathcal{G}(\phi_{11}^N, \varphi_1^N), \varphi_1^{*N} \right).\end{aligned}$$

In the following subsection, we report the numerical results and discuss the physical implications.

5.2 Numerical results and physical implications

5.2.1 Periodic orbit in case of continuous transition

According to the transition Theorem 4.1, in case of $\text{Re}P = P_1 < 0$ the nonlinear system (2.4) undergoes a continuous transition at R^* and the new state ψ_{new} can be approximated by

$$\psi_{new} = \psi_s + \left(\frac{\beta_{11}}{|P_1|} \right)^{\frac{1}{2}} \left(e^{i\beta_{12}t} \phi_1 + e^{-i\beta_{12}t} \overline{\phi_1} \right) + o\left(\beta_{11}^{\frac{1}{2}} \right), \quad (5.10)$$

which is the superposition of the basic steady-state (the Munk profile) and the bifurcated time-periodic solution for $R > R^*$ and $\frac{R-R^*}{R} \ll 1$. Formula (5.10) provides a new effective method for capturing the bifurcated periodic flow, in comparison to the traditional numerical bifurcation theory where one has to solve the nonlinear system up to long time to find the stable bifurcated solution.

For the purpose of illustration of the structure of the bifurcated periodic flow, we take $b = 10\pi$ and $S = 0.2$, then we find that the corresponding critical Reynolds number takes the value $R^* = 30.71255$. Taking $R = 32.71255$, the structure of the bifurcated solution ψ_{new} in a period $T = 89.6809$ is displayed in Fig. 5.

Observing from (a)-(b) in Fig. 5, one sees that the periodic flow given by (5.10) moves in the y -direction, with two (counterclockwise) vortices close to the boundary $x = 0$. We point out that the magnitude of the bifurcated limit cycle grows with the square root of the difference $R - R^*$ which is illustrated in Fig. 3.

5.2.2 Effect of stratification and aspect ratio on types of transition

In earlier numerical investigation of instabilities associated with the western boundary current such as that in [3], only supercritical Hopf bifurcation (continuous transition in

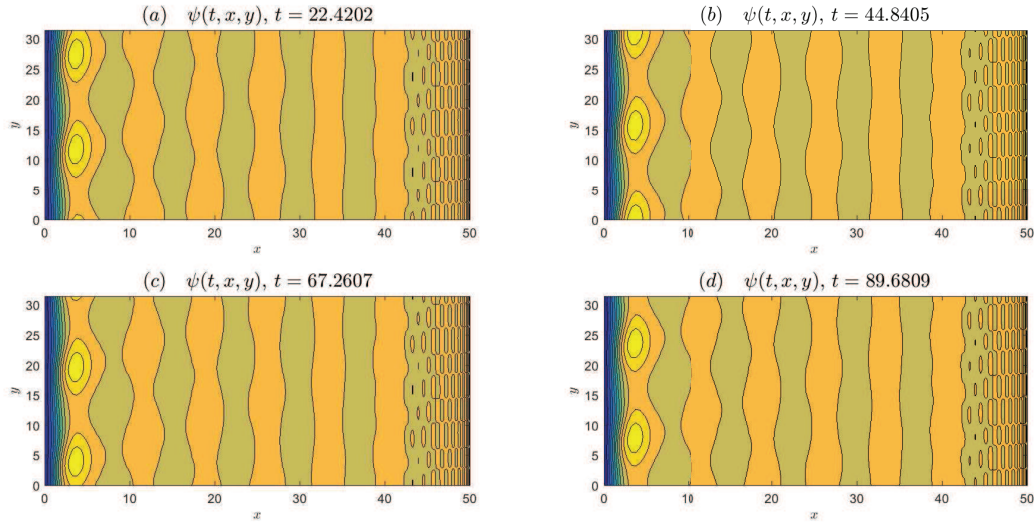


Figure 5: The evolution of the periodic solution with $b = 10\pi$, $R = 32.71255$ at period $T/4$ (a), $2T/4$ (b), $3T/4$ (c) and T (d).

the language of dynamic transition) is discovered and the effect of the aspect ratio is often overlooked. As stated in the transition Theorem 4.1, the types of transition that the nonlinear system (2.4) undergoes at the critical Reynolds number R^* can be either continuous or catastrophic, and which type occurs is uniquely determined by the sign of the real part of the transition number P , cf. (4.17). In this section, we calculate numerically the value of the transition number for $S \in [0, 0.8]$ and $\alpha \in [0.1, 0.5]$ as used in [3]. We shall show that the dynamical system can indeed undergo a catastrophic transition (subcritical Hopf bifurcation).

Here we take $a = 50$, $\alpha \in (0.1, 0.5)$ and $S \in \{0, 0.2, 0.4, 0.6\}$, we compute the corresponding values of the real part of P which are shown in Fig. 6. One observes that for small stratification number $0 < S \ll 1$ the corresponding transition number $\text{Re}P$ is negative for all $\alpha \in [0.1, 0.5]$, i.e., the type of transition is continuous in this parameter range. In this case, there exists a periodic orbit as the Reynolds number R crosses the respective critical value R^* . On the other hand for $S = 0.6$ and $0.25 \leq \alpha < 0.4$, the transition number $\text{Re}P$ is positive. Hence, two types of transition can happen for the system (2.4).

Fig. 6 shows that the types of transitions, being continuous or catastrophic, for the nonlinear system (2.4) at the critical Reynolds number, depend critically on the combination of stratification S and aspect-ratio α . It appears that the system favours continuous transition in the sense that continuous transition occurs for the majority of the parameter values, which to some extent explains why only supercritical Hopf bifurcations are observed in earlier numerical studies. In Fig. 7 we delineate the regions separating the continuous and catastrophic transitions in the $S - \alpha$ parameter plane with $0 < S < 0.8$ and $0.1 < \alpha < 0.65$. It is shown that the plane is separated by a discontinuous curve into two re-

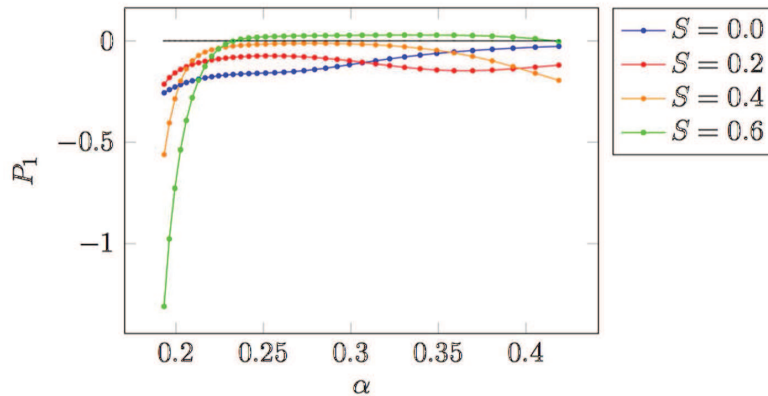


Figure 6: The values P_1 of the real part of the transition number as a function of the aspect ratio α and stratification S . Positive values indicate a catastrophic transition; negative values imply continuous transition.

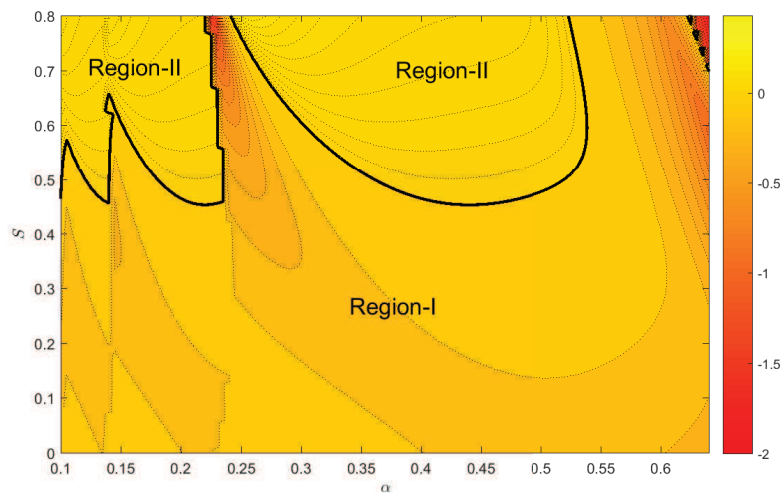


Figure 7: Regions separating the two types of transition: Region-I, continuous transition; Region-II, catastrophic transition.

gions: Region-I where continuous transition occurs, and Region-II in which catastrophic transition happens.

Our analysis and numerical results reveal the loss of stability of the western boundary current is associated with oscillatory instability. The mechanisms for the oscillatory instability are intrinsically different: in the case of continuous transition (supercritical Hopf bifurcation) a stable periodic orbit bifurcates from the steady-state solution and grows continuously as the Reynolds number increases; whereas in the case of catastrophic transition an unstable limit cycle occurs before the Reynolds number reaches its threshold, and no new periodic orbits bifurcate from it after the loss of stability of the basic flow.

The type of transition responsible for the instability depends on the stratification and the aspect ratio. Although these conclusions are drawn for the somewhat simpler one-layer quasi-geostrophic potential vorticity equation when the aspect ratio is small, they provide further insight into the complex instabilities of the western boundary current and general circulation models.

6 Conclusion

In this article we study analytically and numerically the instabilities of the western boundary current governed by the quasi-geostrophic potential vorticity equation in a rectangular closed basin. By reducing the infinite dynamical system to a finite dimensional one via center manifold reduction, we derive a non-dimensional transition number whose sign determines the types of dynamic transition. We show by careful numerical evaluation of the transition number that both continuous transitions (supercritical Hopf bifurcation) and catastrophic transitions (subcritical Hopf bifurcation) can happen at the critical Reynolds number, depending on the aspect ratio and the stratification. Our results give a complete characterization of the instability mechanism of the western boundary current in the QG setting. Our method is useful for the study of instabilities and transitions in general circulation models.

Acknowledgments

The work of Daozhi Han is supported by a seed fund of the Material Research Center at Missouri University of Science and Technology; Marco Hernandez was supported in part by the National Science Foundation (NSF) grant DMS-1515024, and by the Office of Naval Research (ONR) grant N00014-15-1-2662; Quan Wang was supported by the NSFC (No. 11771306). The authors thank Dr. Shouhong Wang and Dr. Taylan Sengul for helpful discussions in the preparation of the article.

References

- [1] Pavel S. Berloff and James C. McWilliams. Quasigeostrophic dynamics of the western boundary current. *Journal of Physical Oceanography*, 29(10):2607–2634, 1999.
- [2] S. P. Berloff, P. Meacham. The dynamics of an equivalent-barotropic model of the wind-driven circulation. *Journal of Marine Research*, 55(3):407–451, 1997.
- [3] S. P. Berloff, P. Meacham. On the stability of the wind-driven circulation. *Journal of Marine Research*, 56(5):937–993, 1998.
- [4] Kirk Bryan. A numerical investigation of a nonlinear model of a wind-driven ocean. *Journal of the Atmospheric Sciences*, 20(6):594–606, 1963.
- [5] Zhi-Min Chen, Michael Ghil, Eric Simonnet, and Shouhong Wang. Hopf bifurcation in quasi-geostrophic channel flow. *SIAM J. Appl. Math.*, 64(1):343–368, 2003.

- [6] Zhi-Min Chen and W. G. Price. Bifurcating periodic solutions of the wind-driven circulation equations. *J. Math. Anal. Appl.*, 304(2):783–796, 2005.
- [7] Henk Dijkstra, Taylan Sengul, Jie Shen, and Shouhong Wang. Dynamic transitions of quasi-geostrophic channel flow. *SIAM J. Appl. Math.*, 75(5):2361–2378, 2015.
- [8] Henk A. Dijkstra and Michael Ghil. Low-frequency variability of the large-scale ocean circulation: A dynamical systems approach. *Reviews of Geophysics*, 43(3):n/a–n/a, 2005. RG3002.
- [9] P. G. Drazin and W. H. Reid. *Hydrodynamic stability*. Cambridge Mathematical Library. Cambridge University Press, Cambridge, second edition, 2004. With a foreword by John Miles.
- [10] Michael Ghil. The wind-driven ocean circulation: applying dynamical systems theory to a climate problem. *Discrete Contin. Dyn. Syst.*, 37(1):189–228, 2017.
- [11] G. R. Ierley and W. R. Young. Viscous instabilities in the western boundary layer. *Journal of Physical Oceanography*, 21(9):1323–1332, 1991.
- [12] Caroline A. Katsman, Sybren S. Drijfhout, and Henk A. Dijkstra. The interaction of a deep western boundary current and the wind-driven gyres as a cause for low-frequency variability. *Journal of Physical Oceanography*, 31(8):2321–2339, 2001.
- [13] Sang-Ki Lee. On the structure of supercritical western boundary currents. *Dynamics of Atmospheres and Oceans*, 33(4):303 – 319, 2001.
- [14] Honghu Liu, Taylan Sengul, and Shouhong Wang. Dynamic transitions for quasilinear systems and Cahn-Hilliard equation with Onsager mobility. *J. Math. Phys.*, 53(2):023518, 31, 2012.
- [15] Honghu Liu, Taylan Sengul, Shouhong Wang, and Pingwen Zhang. Dynamic transitions and pattern formations for a Cahn-Hilliard model with long-range repulsive interactions. *Commun. Math. Sci.*, 13(5):1289–1315, 2015.
- [16] Tian Ma and Shouhong Wang. Rayleigh-Bénard convection: dynamics and structure in the physical space. *Commun. Math. Sci.*, 5(3):553–574, 2007.
- [17] Tian Ma and Shouhong Wang. Boundary-layer and interior separations in the Taylor-Couette-Poiseuille flow. *J. Math. Phys.*, 50(3):033101, 29, 2009.
- [18] Tian Ma and Shouhong Wang. *Phase transition dynamics*. Springer, New York, 2014.
- [19] A. Majda and X. Wang. *Nonlinear Dynamics and Statistical Theories for Basic Geophysical Flows*. Cambridge University Press, 2006.
- [20] Walter H. Munk. On the wind-driven ocean circulation. *Journal of Meteorology*, 7(2):80–93, 1950.
- [21] Saadet Özer and Taylan Sengül. Stability and transitions of the second grade Poiseuille flow. *Phys. D*, 331:71 – 81, 2016.
- [22] J. Pedlosky. *Geophysical Fluid Dynamics*. Springer, New York, 1979.
- [23] Taylan Sengul, Jie Shen, and Shouhong Wang. Pattern formations of 2D Rayleigh-Bénard convection with no-slip boundary conditions for the velocity at the critical length scales. *Math. Methods Appl. Sci.*, 38(17):3792–3806, 2015.
- [24] Taylan Sengul and Shouhong Wang. Pattern formation in Rayleigh-Bénard convection. *Commun. Math. Sci.*, 11(1):315–343, 2013.
- [25] James Serrin. On the stability of viscous fluid motions. *Arch. Rational Mech. Anal.*, 3:1–13, 1959.
- [26] Jie Shen, Tao Tang, and Li-Lian Wang. *Spectral methods: algorithms, analysis and applications*, volume 41. Springer Science & Business Media, 2011.
- [27] Eric Simonnet, Michael Ghil, Kayo Ide, Roger Temam, and Shouhong Wang. Low-frequency variability in shallow-water models of the wind-driven ocean circulation. part i: Steady-state

- solution. *Journal of Physical Oceanography*, 33(4):712 – 728, 2003.
- [28] H. Stommel. *The Gulf Stream: A Physical and Dynamical Description*. California library reprint series. University of California Press, 1965.
- [29] George Veronis. Wind-driven ocean circulation—part 1. linear theory and perturbation analysis. *Deep Sea Research and Oceanographic Abstracts*, 13(1):17 – 29, 1966.
- [30] George Veronis. Wind-driven ocean circulation—part 2. numerical solutions of the non-linear problem. *Deep Sea Research and Oceanographic Abstracts*, 13(1):31 – 55, 1966.
- [31] Quan Wang. Stability and bifurcation of a viscous incompressible plasma fluid contained between two concentric rotating cylinders. *Discrete Contin. Dyn. Syst.-B*, 19(2):543 – 563, 2014.